

BIOLOGICAL TRANSLATION: BIOLOGICAL MATERIALS SCIENCE AND BIOINSPIRED DESIGN

Enhancement of Biocompatibility of Fish Scale-Based Hydroxyapatite-Infused Fibrous Scaffolds by Low-Temperature Plasma

DEEPA KODALI, 1,2 ZAHEERUDDIN MOHAMMED, 1 DILIP REDDY GUNTURU, 3 TEMESGEN SAMUEL, 3 SHAIK JEELANI, 1 and VIJAYA K. RANGARI $^{\rm D}$ 1,4

1.—Department of Materials Science Engineering, Tuskegee University, AL 36088, USA. 2.—Department of Mechanical Engineering, Christian University, Memphis, TN 38104, USA. 3.—Department of Biomedical Sciences, Tuskegee University, Tuskegee, AL 36088, USA. 4.—e-mail: Vrangari@tuskegee.edu

Owing to its excellent ability to enhance the cell growth and proliferation, hydroxyapatite (HAp) has received tremendous attention as a highly valuable biomaterials. Byproducts from the marine environment, especially fish scales, have proved to be a vital source for HAp. Nevertheless, HAp still has a profound influence on the matrices designed for biomedical applications. In this study, fish scale-derived nano-hydroxyapatite (n-HAp) = infused non-woven polycaprolactone (PCL) fibrous scaffolds are developed byforce spinning. The surface properties of the nanofibrous scaffolds are modified by oxygen plasma treatment, and their influence on n-HAP-infused PCL scaffolds is investigated. Plasma treatment is favorable for 2 wt.% and 3 wt.% scaffolds with a high O/C ratio and improving C=O content, and are found to have high cell growth. The 3 wt.% scaffolds have high crystallinity which is twice the crystallinity of neat fibers. The plasma treated 2 wt.% and 3 wt.% scaffolds were found to have high cell growth almost twice that of neat scaffolds, and these observations complied with the results from x-ray photoelectron spectroscopy (XPS). The plasma treatment enhances the functional properties and biocompatibility of fibrous scaffolds containing 2 and 3 wt.% n-HAP.

INTRODUCTION

Bone regeneration plays a crucial role in the repair and regeneration of bones that are disintegrated or damaged due to various reasons, such as injury, disease, or trauma. 1,2 Although conventional techniques, such as auto and allograft bones and demineralized bones used for the treatment of bones, the limitations and complexities associated with these techniques have forced the scientists to seek alternatives for bone replacements.³ Consequently, tissue engineering (TE) has emerged as a promising alternative for the regeneration of damaged tissues by implementing various strategies,

such as transplantation of cells, inducing growth factors such as peptides at anticipated sites, and the use of three-dimensional (3D) extracellular matrix (ECM) scaffolds for cell growth and adherence.¹ Given that cell proliferation and differentiation are the key objectives of TE, a quintessential TE scaffold should be porous, with appropriate biological, mechanical, and physical properties.^{2,4,5} The desired features of the scaffolds are substantially influenced by the materials and the fabrication techniques. Several fabrication techniques, such as freeze drying, 6 solvent casting, 7 gas foaming, 8 particulate leaching, 9 and rapid prototyping 10 have been employed to fabricate TE scaffolds with adequate mechanical and biological properties. Nevertheless, biomimicking natural ECM scaffolds with an ideal material with excellent regeneration properties is still a challenge.

(Received September 11, 2022; accepted February 20, 2023)

Published online: 22 March 2023

Over the past few decades, efforts have been made to develop bioactive and biocompatible fibrous TE scaffolds with interconnected porosity to improve cell adhesion and proliferation. 1,5 Electrospinning, 11,12 phase separation, 13 molecular assembly, 14 and 3D printing 15 are a few methods to obtain porous scaffolds. Owing to the biodegradability and high porosity, microfibrous scaffolds obtained by electrospinning have become noteworthy in bioengineering. 16 However, despite several advantages, the small pore size and the thickness of the electrospun layers limit their use in the development of 3D scaffolds.¹⁷ On that account, force spinning, which uses centrifugal forces to generate fibers, has emerged as a novel alternative to electrospinning. 18-20 Force spinning can successfully generate micro- and nanofibrous scaffolds with suitable thicknesses, allowing them to have deep cell penetration, and thus has huge potential for TE applications. 17 Among various polymers, aliphatic polyesters, such as polyglycolide, polylactide, polycaprolactone (PCL), and poly(L-lactide), are widely used for TE applications. Among these polymers, PCL has become the preferred source for biomedical applications in view of its superior mechanical properties and excellent biocompatibility and biodegradability.^{21–24} This aliphatic polyester's semi-crystalline and non-toxic nature makes it ideal for the fabrication of scaffolds for TE, drug delivery, sutures, and bone repairs.²

In addition to the fabrication techniques, biomaterials used for developing scaffolds also play a crucial role in obtaining the desired properties of the scaffolds. Polymer composites reinforced with bioceramics offer novel composites with enhanced thermo-mechanical and biological properties. 1,26,27 Because of their appealing biodegradable, bioactive, and osteoconductive properties, as well as their remarkable ability of bonding with bone, bioceramics, such as calcium phosphate, calcium sulfate, β -TCP, and hydroxyapatite (HAp), are widely used in clinical applications, such as implant coatings and fillers for bone voids. 28 Calcium apatite-based ceramic powders, when blended with polymers having adequate cell adhesion capability, will increase the surface hydrophilicity and cell affinity while retaining the mechanical strength.^{29,30} HAp [Ca₁₀(PO₄)₆(OH)₂] is one such calcium phosphate having s Ca/P ratio of 1.67 and a chemical composition similar to that of minerals existing in bone and tooth enamel. 31,32 As such, various biomedical applications, such as coatings, TE, scaffolds, biogenic catalysis, orthopedics, and odontology for repairs and regenerations, have considered bioceramic HAp as a promising material. 32,33 Thus, HAp an efficient scaffold material possessing notable bioactive, osteoconductive, and biocompatible properties, besides being non-toxic and noninflammatory while promoting cell colonization and reformation. 25,34,35

HAp has been synthesized from various natural waste resources, such as seashells, ^{36,37} eggshells, ³⁷ and fish scales. ^{38,39} Large amounts of waste shells that are being discarded after utilization directly contribute to land and air pollution during their decay. 40,41 Especially, massive amounts of waste fish byproducts (approximately 18–30 million tons) are being disposed globally, 8% of which are fish scales, thus encouraging researchers to investigate ways to reutilize this bio-waste. 42 HAp is one of the primary constituents of fish scales and the HAp extracted from them is spherical, biocompatible, and bioactive. The HAp derived from the whitemouth croaker (Micropogonias furnieri) has been shown to be highly biocompatible when a rat subcutaneous tissue test was performed. 46 Several researchers have shown that fish scale-derived HAp is bioactive and can be successfully used for developing scaffolds for TE applications. 47–55

Further, to remove the inhibitions of the cell attachment on the polymer surface, surface modifications have been employed to enhance the wettability, surface free energy, and biocompatibility of the polymers. ⁵⁶ Plasma treatment is one such surface modification which is very efficient in meliorating the biological properties, while leaving the other desired properties unaffected.²⁴ Oxygen plasma treatment of PCL polymer has been shown to enhance the surface properties by replacing weak chemical bonds on the surface by highly reactive amine, carboxyl, hydroxyl, and aldehyde groups.²⁴ The oxygen plasma treatment of calcium carbonate (CaCO₃)-coated PCL scaffolds has resulted in the nucleation and precipitation of CaCO3 deep inside the porous structure, thus making it suitable for drug delivery systems. ²³ The oxygen and ammonia plasma treatment improves the adhesion and proliferation of human umbilical endothelial cells on PCL scaffolds.⁵⁷ PCL/HAp nanofibrous scaffolds were modified using oxygen plasma treatment, which helped in the significant growth of human fetal osteoblast cells.⁵⁸ The oxygen plasma treatment improved the roughness and wettability of 3Dprinted HAp/gelatin/chitosan composite scaffolds and also showed improved cell proliferation.⁵⁹ More recently, Asadian et al. plasma-treated a PCL solution before generating nanofibers, observing a strong influence of the pretreatment on the morphology of the electrospun PCL nanofibers. The enhancements were attributed to the higher solution conductivity, a parameter that contributes to process improvement.

In our previous work, the influence of fish scale-based HAp on the thermo-mechanical and biological properties of force-spun PCL scaffolds infused with nano-HAp derived from freshwater carp (*Labeo catla*) and deep-sea pink perch (*Nemipterus japonicus*) fish scales were investigated. Synthesis of HAp from the fish scales using a low-cost yet sophisticated method was described in detail, and the characterization results of HAp were included in

the supplementary materials. The present study is an extension of our previous work to optimize the performance of PCL fibrous scaffolds infused with carp HAp. In our present work, in order to further optimize the performance of the PCL scaffolds, surface modification has been performed by oxygen plasma treatment, and the thermal and biological properties of the modified scaffolds have been analyzed. It is also to be noted that, in our present study, 14 wt.% of PCL has been used with chloroform as the solvent, whereas in our previous work we used 16 wt.% of PCL with tetrahydrofuran and chloroform (70:30 wt/wt) as solvent. Although numerous reports have been provided for the plasma treatment of PCL and PCL/HAp scaffolds, to the best of our knowledge none of the studies has thus far reported the analysis of plasma-modified force-spun PCL scaffolds infused with fish scalederived HAp.

EXPERIMENTAL

Materials

The force-spun composite fibers were developed using powdered PCL with a molecular weight of 50,000 (Polysciences, Warrington, PA, USA). Chloroform with ACS reagent \geq 99.8% was purchased from Sigma-Aldrich (St. Louis, MO, USA) and has been used to dissolve the PCL.

The raw fish scales of the carp, which were cleaned and sun-dried, were acquired from Nizona, Mumbai, India. They contained 20–30% of moisture. Calcination of these scales was performed in a box furnace for 3 h at 800°C. Using a mortar and pestle, the calcined powder was ground into a fine powder. To further reduce the size of the powder, the calcined powder was nanomilled in an MTI compact nanoagitator bead mill for 1 h at 2000 rpm using 0.3-mm zirconia balls. The loaded powder to ball ratio was 3:7 with distilled water as a solvent to dissipate the heat from the milling process. The powder was centrifuged using a Beckman Coulter Allegra X-30 R centrifuge to separate the nanohydroxyapatite (n-HAp) particles. These were then dried, ground with a mortar and pestle, and stored for further use.

Force-Spinning of Fibers

The polymer solution for force-spinning of the fibers was prepared by dissolving 14 wt.% of powdered PCL in chloroform. To obtain a homogenous solution, the PCL solution was magnetically stirred continuously for 3 h at 170 rpm. The evaporation of the solvent was prevented by sealing the vials during the stirring process. The synthesized n-HAp powder was then added to the PCL solution in by 2, 3 and 5 wt.%. A planetary non-contact Thinky ARE-250 mixer, was used to mix the solution thoroughly for 7 min at 1900 rpm for homogenous dispersion of the n-HAp particles.

Nonwoven fibrous mats from the polymer solution mixture were obtained using a Force-pinning Cyclone L-1000 M apparatus (Fiberio) equipped with a solution spinneret. A 24-ga $\times \frac{1}{2}$ " stainless steel regular bevel needle was anchored to the spinneret to dispense the polymer jet. A 2-ml amount of the precursor (PCL-n-HAp) solution was administered into the spinneret using a pipette. The spinneret angular velocity was maintained at 6000 rpm with a spin time of 10 min. The fibers were collected on the collector equipped with equally spaced vertical plates. The collector plates were placed at a distance of 115 mm from the needle (190 mm from the center of the spinneret). The studies by Kodali et al. provide a detailed description of the set-up. 40,61 The collected fibers were stored under desiccation for further characterization.

Plasma Treatment of Fibers

The force-spun fibers were subjected to low-temperature plasma treatment using Plasma Etch's PE-100 equipment. To ensure consistent functionalization of the samples, the machine's design was customized to include a spinning circular drum as a sample container. The PCL mats were plasmatreated in the presence of oxygen gas at a steady flow of 30 ml for 5 min at 150-W RF radiation generated at a standard frequency of 13.5 MHz. The surface-treated PCL scaffold mats were then used for characterization and cell adhesion analysis.

Fiber Characterization

X-Ray Diffraction (XRD)

X-ray diffraction studies were carried out using a Bruker D8 diffractometer (DMAX2100) equipped with monochromatic Cu K α radiation. This was operated at a scan rate of 1°/min, with a step size of 0.02°, varying from 10° to 90° Bragg's angle of diffraction at 45 kV and 40 mA.

X-Ray Photoelectron Spectroscopy (XPS)

The surface analysis of the synthesized nanomilled HAp powder was analyzed using XPS. A Versaprobe 5000 XPS instrument (Phi Electronics) equipped with a monochromatic X-ray source at 4.4 W with a spot size of 20 μ m was used to perform the analysis. The system also offers dual neutralization, eliminating the need for correction of the peak positions. A pass energy of 187.85 eV with a step size of 0.8 eV was used to perform the survey scan. The angle between the surface normal and analyzer lens axis was maintained at 45° to acquire the data. This angle is also known as the photodetector takeoff angle.

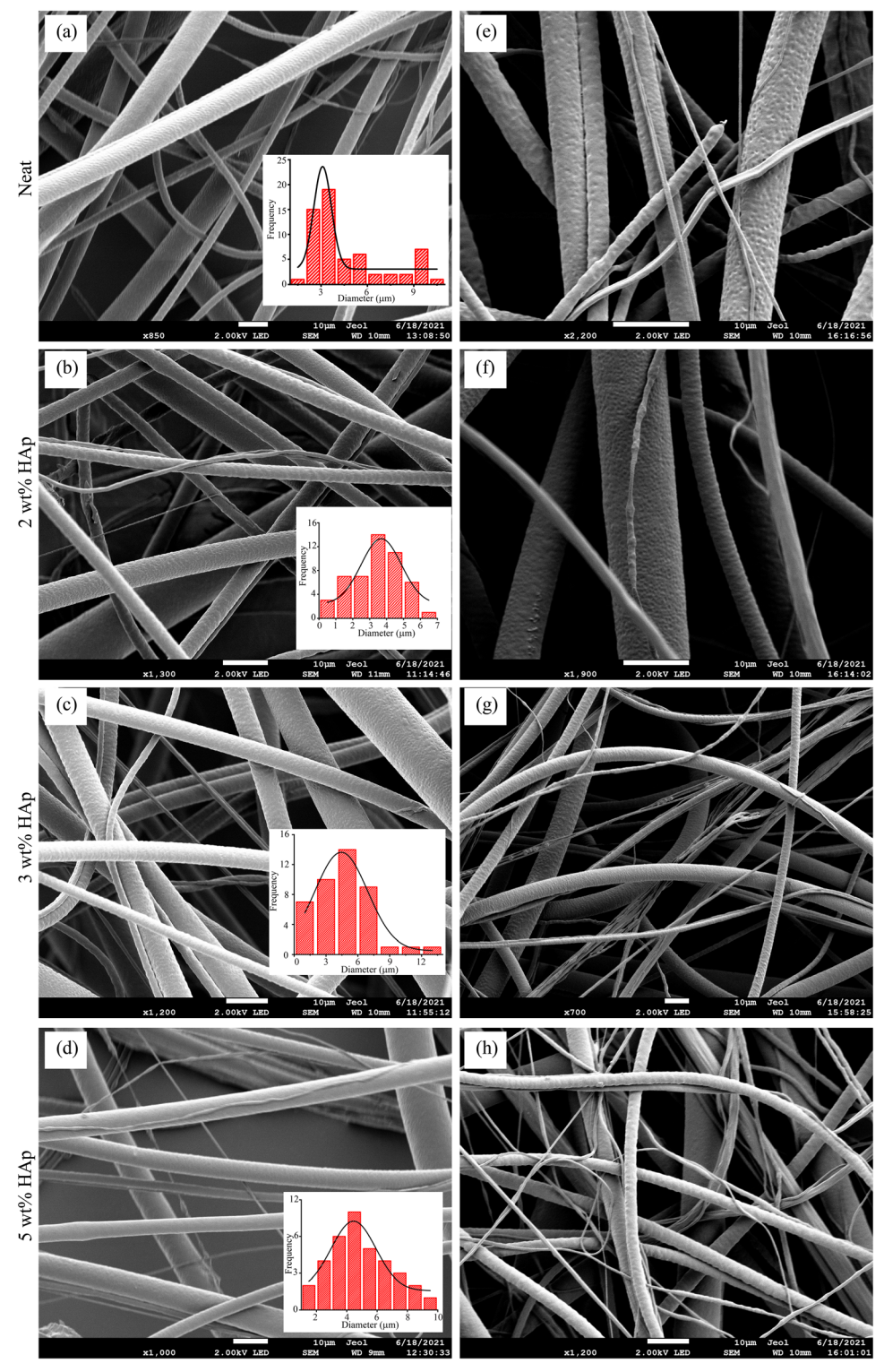


Fig. 1. SEM micrographs of PCL-n-HAp fibers with corresponding histograms showing fiber diameter distribution for (a) neat, (b) n-HAp 2 wt.%, (c) n-HAp 3 wt.%, (d) n-HAp 5 wt.%, (e) plasma-treated neat (f) plasma-treated n-HAp 2 wt.%, (g) plasma-treated n-HAp 3 wt.%, and (h) plasma-treated n-HAp 5 wt.%.

Scanning Electron Microscopy (SEM)

A JSM-7200F field-emission scanning electron microscope (FESEM; JEOL, Peabody, MA, USA) at

2 kV was used to examine the morphology of the synthesized n-HAp particles and the PCL-n-HAp fibers. Gold/palladium (Au/Pd) was sputtered onto

the samples for 3 min at 10 mA using a Hummer sputter coater.

Thermogravimetric Analysis (TGA)

A TA Q500 Thermogravimetric Analyzer was used to perform the TGA. The weight change of the specimens obtained with the increase in temperature was used to estimate the decomposition temperature, weight change, and the residue. An approximately 15-mg sample was placed on a platinum pan for analysis. A ramp rate of 10 °C/min was used to heat the sample from 30°C to 800°C under nitrogen.

Differential Scanning Calorimetery (DSC)

DSC was used to analyze the thermal properties of the fibers. A DSC TA-Q series 2000 equipment was used for the test, and samples weighing 10–12 mg sealed in hermetic pans were analyzed. The DSC analysis was performed from -80°C to $+80^{\circ}\text{C}$ followed by cooling to -80°C and then heating up to $+80^{\circ}\text{C}$ with ramp rate of 5°C/min under nitrogen flow.

Cell Adhesion

The adaptability of the n-HAp PCL scaffolds for cell adhesion and proliferation were determined using human osteoblast cells (hFOB; American Type Culture Collection #CRL-11372). Untreated (UT) and plasma-treated (PT) PCL scaffolds of 2, 3, and 5 wt.% along with neat scaffolds were studied for various times for cell adhesion and growth. The hFOB cells were grown in media composed of Dulbecco's Modified Eagle Medium–High Glucose

containing 1% (v/v) bovine serum, L-glutamine, and $10~\mu g/mL$ ciprofloxacin (antibacterial). A humidified incubator under normal cell culture conditions (37 °C, 5% CO2/95% air environment) was used to incubate the cells. All the scaffolds were first sterilized in 70% ethanol for 30 min, and then washed three times with phosphate buffered saline before seeding with the cells. Each scaffold was seeded with hFOB cells at the rate of 1×10^4 cell per each scaffold in a sterile 24-well plate. Initially, the cells were dispensed in $100~\mu L$ of medium, spread over each scaffold and kept for 30 min for adhesion; later, the remaining medium was added. The seeded scaffolds were incubated as above for different times (3, 4, and 5 days).

Cell Counting and Analysis

For cell counting, each scaffold was studied in triplicate. After each day of treatment, the scaffolds were lifted out of the plate and the cells were fixed with ascending grades of alcohol followed by staining with 1 μ g/mL of 4′,6-diamidino-2-phenylindole (DAPI) solution. The stained scaffolds were examined under a fluorescence microscope (Olympus-SZX16) with an Olympus SDF PLAPO objective (1.6XPF). Photomicrographs were captured by a digital camera (DP74, Olympus) using cellSens software (Olympus). The NIH software ImageJ was used for cell counting. Automated counting of single-color images was performed, and three counts per each scaffold were recorded.

The cell counts were analyzed per day and per treatment by applying analysis of variance (ANOVA). IBM-SPSS (v. 26) was used for the performing of ANOVA. The significance level was

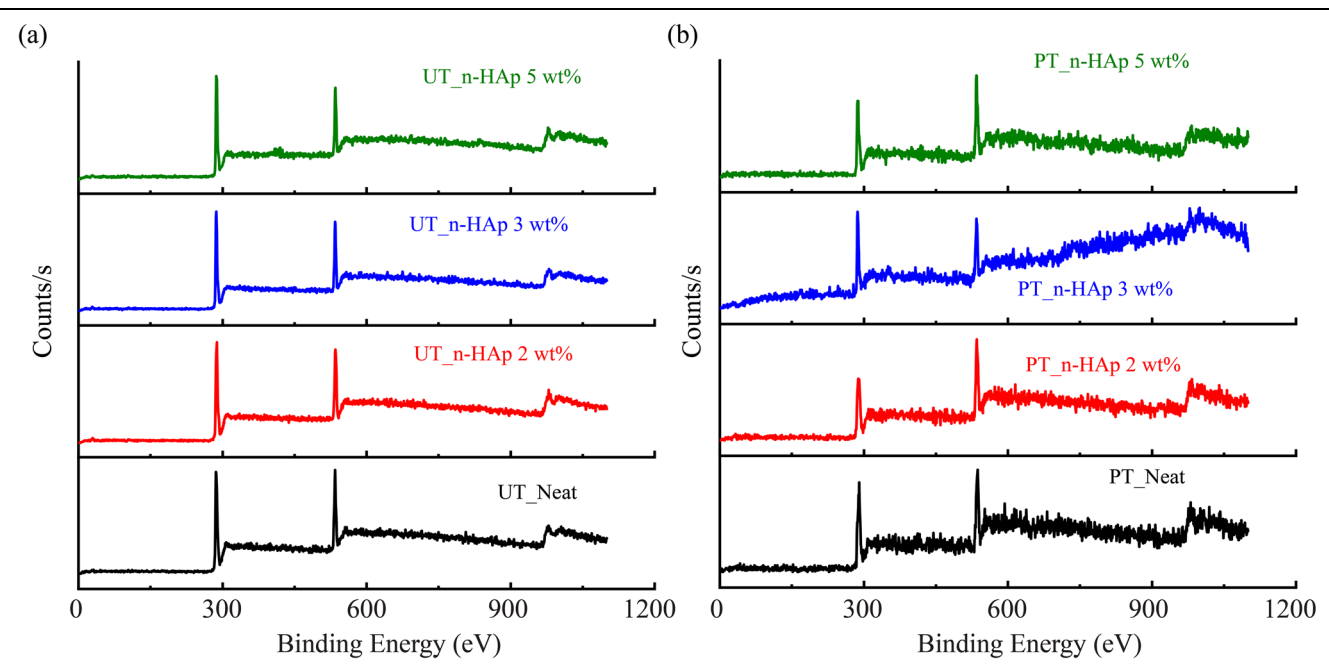


Fig. 2. XPS spectra of (a) untreated (UT) and (b) plasma treated (PT) n-HAp PCL fibers with 2, 3, and 5 wt.%.

Table I. Elemental composition,	O/C ratios, and relative areaa	(%) corresponding to different chemical bonds
	- · · · · · · · · · · · · · · · · ·	· (/-/ /-

Treatment	%C	%O	\mathbf{O}/\mathbf{C}	$\mathbf{C}\text{-}\mathbf{C}$	C-O	C=O
UT neat	74.7	25.3	0.34	50.04	35.07	14.89
PT_neat	71.6	28.4	0.39	37.22	48.17	14.61
UT_n-HAp 2 wt.%	76.3	23.7	0.31	30.28	56.25	10.63
PT_n-HAp 2 wt.%	68.8	31.2	0.45	17.02	56.28	26.71
UT_n-HAp 3 wt.%	77.5	22.5	0.29	45.88	34.55	7.54
PT_n-HAp 3 wt.%	71.0	29.0	0.41	25.44	64.22	10.34
UT_n-HAp 5 wt.%	76.5	21.3	0.27	37.41	47.13	10.34
PT_n-HAp 5 wt.%	71.6	28.4	0.39	37.76	36.80	25.43

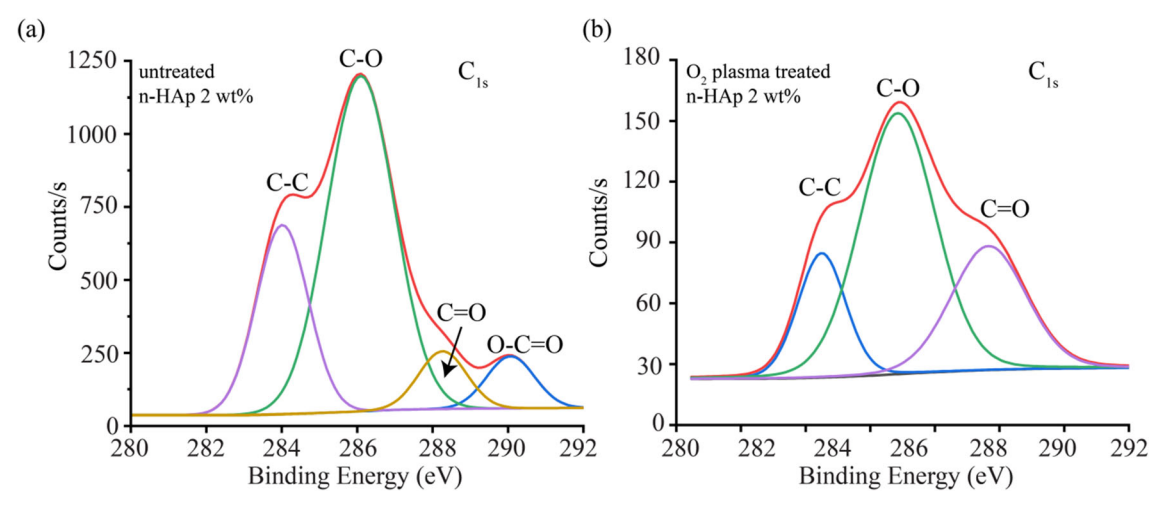


Fig. 3. Deconvoluted graphs of (a) untreated (UT) and (b) plasma-treated (PT) n-HAp 2 wt.% PCL fibers of high resolution C_{1s}.

kept at p < 0.05 and Tukey's HSD (honest significant difference) post hoc test was performed for comparing the differences between the treatment groups.

RESULTS AND DISCUSSION

Characterization of HAp Powder

The synthesized HAp powder was analyzed using XRD, XPS, SEM, and TEM, and the descriptions of the same are presented in the online electronic supplementary material (Figures S1, S2, and S3). The characterization results were similar to the results that were presented in our previous work, 60 showing that the synthesized powder conforms to HAp and is nanosized.

Characterization of PCL-n-HAp Fibers

Morphology of Fibers

The analysis of the n-HAp powder synthesized from the carpa fish scales has shown that it can be successfully reinforced as the filler in the polymer matrix, and can be used for biomedical applications. The synthesized n-HAp powder was infused in 2, 3, and 5 wt.% into PCL solution and was force-spun into fibrous mats. The morphology of these nonwoven fibrous mats was analyzed by SEM. Figure 1

shows the SEM micrographs of the PCL-n-HAp mats which were oriented randomly. The diameter of the 3D mesh of the homogenous fibers was analyzed using ImageJ software and evaluated by using Gaussian distribution. The frequency distribution of the diameters is shown in insets of Fig. 1a-d. The neat PCL fiber was the thinnest one and is shown in Fig. 1a with a diameter of around 3.1 μ m. Figure 1b, c, and d show the PCL fibers with 2, 3, and 5 wt.%, respectively. The diameter of the fibers for the neat, 2, 3, and 5 wt.% are tabulated in Table S1 (refer to online supplementary material). It is observed that, with the increase in the filler content, the diameter of the fibers increased. The diameters of the fibers were observed to be within the range of 3-4.5 um which is high compared to the results obtained by using 16 wt.% of PCL with chloroform and tetrahydrofuran as solvents. Furthermore, these results seem to be within a similar range of diameters (1.5–4 μ m) of the fibers that were obtained by using 16 wt.% PCL and only chloroform as the solvent. 40 The nonuniformity of the fibers increased with the increase in filler content due to increase in the agglomerations. Although the fibers were thick, it was observed that they have a slightly porous texture. This porous texture is enriched when the fibers are subjected to plasma treatment. The oxygen plasmaEnhancement of Biocompatibility of Fish Scale-Based Hydroxyapatite-Infused Fibrous Scaffolds by Low-Temperature Plasma

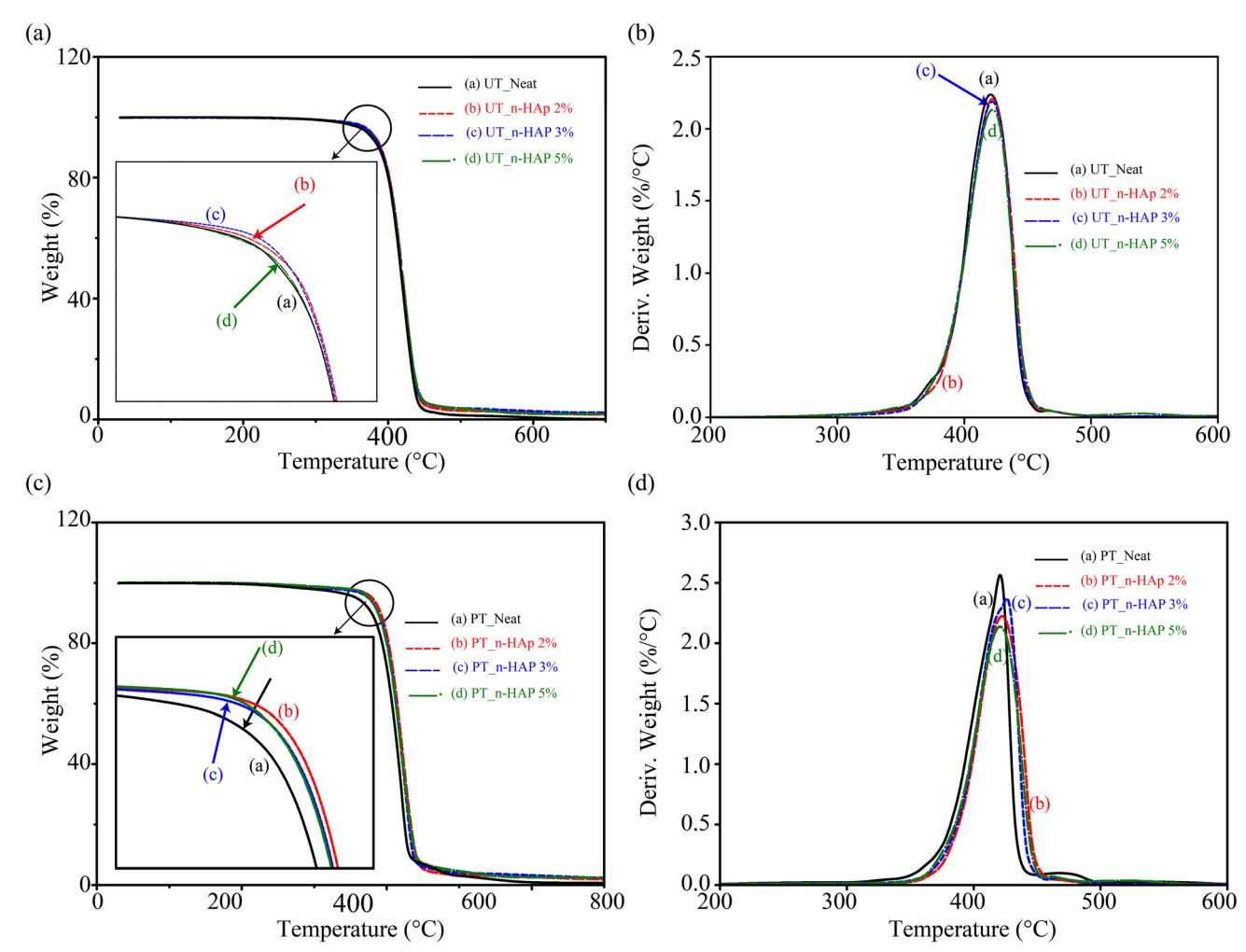


Fig. 4. TGA of untreated and plasma-treated n-HAp PCL fibers showing (a, c) the weight change, and (b, d) the derivative weight change, respectively.

Table II. Summary of the TGA data

n-HAp wt.%	T_i (°C)	T_f (°C)	T_m (°C)	Weight change for T_f (%)	R _{500°C} (%)	R _{650°C} (%)
UT_neat	384.96	440.04	420.73	93.93	1.39	0.27
PT_neat	383.06	430.94	420.83	89.71	3.07	0.74
UT_n-HAp 2 wt.%	386.15	440.81	422.17	90.75	2.90	1.78
PT_n-HAp 2 wt.%	392.67	441.92	422.34	91.51	3.36	2.18
UT_n-HAp 3 wt.%	385.85	440.42	422.11	90.31	3.62	2.35
PT_n-HAp 3 wt.%	387.87	436.93	426.13	90.95	4.09	2.77
UT_n-HAp 5 wt.%	386.41	440.9	422.28	90.11	3.61	1.82
PT_n-HAp 5 wt.%	388.85	438.92	420.79	89.41	4.62	2.52

 T_i initial decomposition temperature, T_f final decomposition temperature, T_m major degradation temperature, $R_{500^{\circ}C}$ residue at 500°C, $R_{650^{\circ}C}$ residue at 650°C.

treated fibers are shown in Fig. 1e, f, g, and h for the neat, 2, 3, and 5 wt.%, respe ctively. The surface roughness of the fibers increased with the plasma treatment, which is evident from the SEM micrographs.

XPS Analysis of Fibers

The surface-binding energies of the oxygen plasma-treated PCL scaffold mats were measured using XPS. Plasma treatments were found to be beneficial in enhancing oxygen-related functional

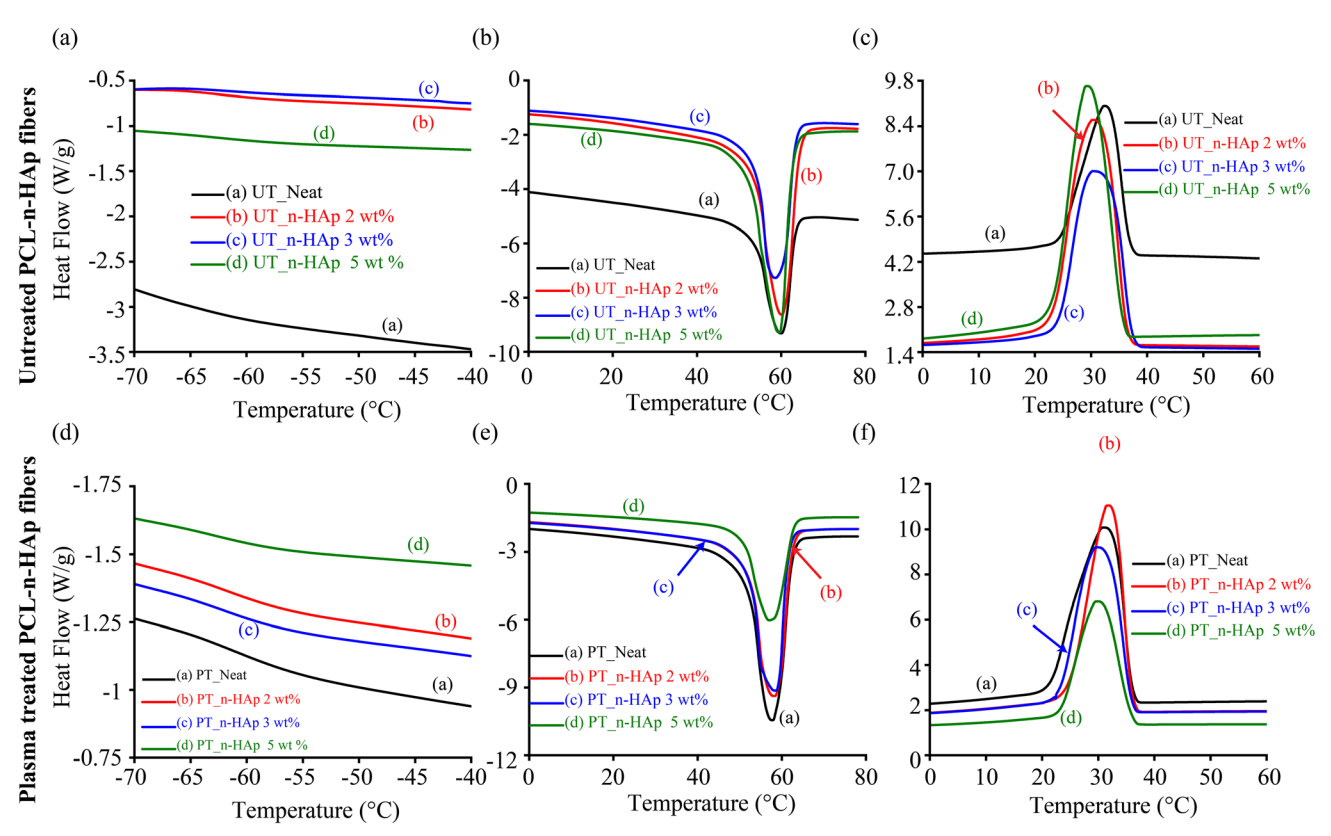


Fig. 5. DSC thermographs showing (a, d) the glass transition temperatures, (b, e) melting endotherms, and (c, f) the crystallization temperatures for untreated and plasma-treated PCL-n-HAp fibers, respectively.

	Table III. DSC anal	lysis of the PCL fibers obtained at various ${f i}$	rotational speeds
--	---------------------	---	-------------------

	Glass transition	First heating	Second	d heating	Со	oling	0/ C4-11
n-HAp wt.%	temperature T_g (°C)	T_m (°C)	T_m (°C)	$\Delta H_m (J/g)$	T_c (°C)	ΔH_c (J/g)	% Crystall- inity (χ_c)
UT_neat	- 63.36	60.68	60.01	57.86	32.47	59.75	1.35
PT_neat	$-\ 61.59$	61.29	57.65	64.15	31.16	65.65	1.08
UT_n-HAp 2 wt.%	$-\ 62.47$	60.46	60.11	55.55	30.45	58.78	2.31
PT_n-HAp 2 wt.%	$-\ 60.9$	59.49	58.32	61.76	31.9	64.81	2.19
UT_n-HAp 3 wt.%	$-\ 61.54$	61.25	58.59	56.43	30.44	60.65	3.02
PT_n-HAp 3 wt.%	$-\ 62.14$	59.42	58.54	64.57	29.67	68.13	2.55
UT_n-HAp 5 wt.%	$-\ 62.4$	60.37	59.42	56.74	29.36	60.23	2.50
PT_n-HAp 5 wt.%	$-\ 62.39$	58.71	57.04	57.74	30.06	60.61	2.05

groups on the scaffold surfaces. The material's hydrophilicity and cell adhesion qualities may be affected by this increase. The surface energy before (a) and after (b) plasma treatments are depicted in Fig. 2. As expected, the samples were dominated by carbon content followed by oxygen. The elemental composition of oxygen, carbon, and the O/C ratio obtained from XPS (Table I) demonstrated a drop in carbon content and an increase in oxygen content after plasma treatment. It can be seen that the plasma-treated PCL fibers with 2 wt.% HAp has the highest oxygen content followed by the 3 wt % HAp

and 5 wt.% HAp. A similar trend was observed for the O/C ratio which was 0.45 for the plasma-treated PCL fibers with 2 wt.% HAp. The O/C ratio of the plasma-treated samples increased by 1.45 times compared to that of the untreated samples. The behavior exhibited by the plasma-treated samples agrees with the results that are reported in the literature. 62

High-resolution C1s spectra were investigated in order to gain a better understanding of the surface functional groups. C-C bonds were approximately 285 eV, C-O bonds were around 286.5 eV, and C=O

bonds were around 289 eV, according to the quantitative results of deconvoluted graphs into the three main sections of the C1s spectra. These results are tabulated in Table I. The concentrations of the functional groups containing oxygen were improved for the fiber samples that were treated with O₂ plasma which might be due to the oxidation of the PCL fiber mat surface. 23,57 The increase in the concentration of oxygen functional groups improvises the hydrophilicity of the surface. It was found that the most reactive C=O bond concentration was highest for 2 wt.% plasma-treated samples. The deconvoluted graphs of the untreated and plasma-treated 2 wt.% samples clearly depict the significant rise in the C=O concentration of the oxygen plasma-treated sample as shown in Fig. 3. It was also observed that the C-O bond is highest for the 3 wt.% plasma followed by the 2 wt.%. Although the C-O bond concentration is highest for the plasma-treated 3 wt.% fiber sample, the C=O concentration also increased when compared to the untreated 3 wt.% sample. This suggests that possibly the 2 wt.% and 3 wt.% loadings are better for oxygen functionalities when plasma-treated and can serve to promote endothelialization, and thus improve cell adhesion and proliferation.

Thermal Analysis of PCL-n-HAp Fibers

The thermal stability, properties, and behavior of the n-HAp PCL fibers were analyzed using TGA and DSC analysis. Figure 4 shows the TGA analysis with a single-step degradation process for both the untreated and plasma-treated fibers, and the results are summarized in Table II. The characteristic weight change and derivative weight change for the untreated fibers are shown in Fig. 4a and b, respectively, while Fig. 4c and d represent the curves for the plasma-treated fibers. A small amount of weight loss (around 2-4%) was observed between 30°C and 350°C which can be attributed to the loss of moisture content. The initial degradation temperatures of the untreated n-HAp PCL fibers increased slightly compared to that of untreated neat fibers. In addition to that, plasma-treated n-

HAp PCL fibers showed a slight increment in the initial degradation temperatures, except for the plasma-treated neat fiber. The final degradation temperatures do not show any change with the increase in filler content for the untreated fibers. However, for the plasma-treated fibers, the final degradation temperature is low compared to the untreated fibers except for the 2 wt.%. The major degradation temperature is higher for the plasmatreated 3 wt.% fibers (426.13°C) compared to all the fibers (Table II). The major degradation temperatures observed are consequent on the C-O content of the fibers.⁶⁴ However, no significant change is observed with the plasma treatment of the fibers. Although not significant, the addition of filler content raised the major degradation by 2°C. The increase in onset temperature and the major degradation suggest that the n-HAP PCL fibers have improved thermal stability compared to the neat fibers by delaying the degradation. The weight loss at the final degradation temperature remains more or less the same without showing any pivotal change. However, the residue was increased for the n-HAP reinforced fibers compared to the neat fibers. The plasma-treated fibers also exhibit a similar behavior. Furthermore, the plasma-treated fibers have more residue at 500°C and 650°C compared to the untreated fibers. Overall, although the plasma treatment of the fibers does not cause any pivotal shift in their thermal stability, it is presumed that, if the plasma treatment parameters are optimized, the thermal stability can be significantly enhanced. Furthermore, the results suggest that the n-HAp PCL scaffolds can be conveniently tailored without incurring any material losses. These results are in agreement with the tensile results that increase in the Young's modulus, as reported in the supplementary material Table S2. The stress-strain curves for the untreated n-HAp PCL are shown in Figure S4 and are discussed in detail in the supplementary material.

In order to further analyze the thermal behavior of the n-HAp PCL fibers, DSC analysis was carried out and the thermographs are shown in Fig. 5. The

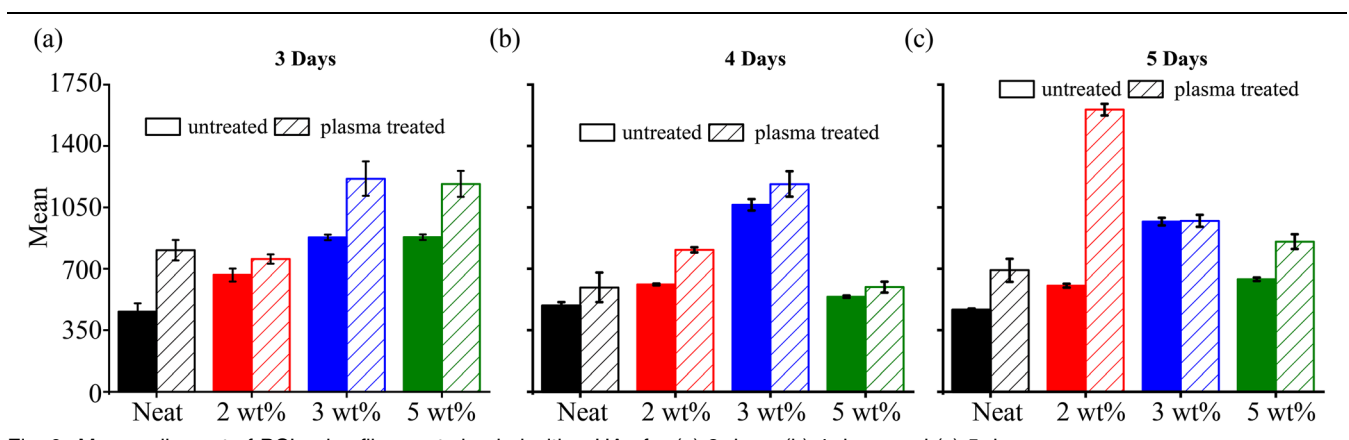


Fig. 6. Mean cell count of PCL microfiber mats loaded with n-HAp for (a) 3 days, (b) 4 days, and (c) 5 days

glass transition (T_g) , crystallization (T_c) , and enthalpy of crystallization (ΔH_c) were evaluated from the first heating curve, whereas the melting (T_m) and the enthalpy of fusion (ΔH_m) were evaluated from the second heating cycle of the DSC endotherms for the untreated and plasma-treated fibers, and are tabulated in Table III. The glass transition temperature has increased with the increase in the filler content and with the plasma treatment of the fiber samples compared to the neat PCL. The addition of n-HAp to the polymer might have restricted the polymer chain mobility, thus increasing T_g .⁴⁰ The plasma treatment of the fibers has also influenced the T_g of the samples, which is evident from the T_g of the plasma-treated neat (-61.59) and 2 wt.% fibers (-60.9). However, as the filler content increases beyond 2 wt.%, the T_g decreases and is also observed to be slightly less than the untreated fibers, which might be due to the agglomerations. Plasma treatment did not result in any focal change in the melting temperature or the crystallization temperature. The crystallinity was calculated from:

$$\chi_c = \frac{\Delta H_m - \Delta H_c}{\Delta H_f},$$

where χ_c is the crystallinity and ΔH_f is the enthalpy of fusion of a 100% crystalline sample (139.5 J/g for PCL). The crystallinity was slightly decreased with the plasma treatment, but the change is not significant. The decreases in the ΔH_m and χ_c suggest that the oxygen plasma treatment resulted in a more amorphous phase in the biopolymers. However, it is observed that crystallization of the n-HAP fibers is more compared to that of the neat fibers for both the untreated and plasma-treated cases. As the filler content increases beyond 3 wt.%, the crystallinity decreases, which might be due to hydrogen bond formation between the PCL and the n-HAp that resulted in the restricted mobility of the polymer chain reducing the crystallinity. He are sufficiently as the crystallinity.

Cell Proliferation Analysis of PCL-n-HAp Fibers

The functionality and the biocompatibility of the force-spun fibrous scaffolds were analyzed by studying the cell adhesion at 3, 4, and 5 days. The DAPI-stained micrographs of the seeded scaffolds that were immersed in culture media for 3, 4, and 5 days for PCL-n-Hap (2%, 3%, and 5%) and -neat fibers were analyzed using ImageJ which was used to obtain the cell count and the mean cell count, by performing ANOVA, as shown in Fig. 6. The mean cell count for each scaffold for different days, including the F value and significance, are presented in Table IV. The neat fibrous scaffolds exhibit significantly lower cell growth throughout the study period. Following seeding of the cells, the smooth surface of the scaffold became coarse, as new

Table IV. Mean cell count of untreated (UT) and plasma-treated (PT) n-HAp PCL scaffolds for 3, 4, and 5 days

	Signif	.003
	\boldsymbol{F}	6.9 256.2 5.8 40.9
L	5 days	$691.67 \pm 64.9 \text{ Aab} \\ 1607.0 \pm 33.0 \text{ Cd} \\ 973.33 \pm 34.0 \text{ Bab} \\ 854.67 \pm 41.9 \text{ ABb} \\ 78.17 \\ .000$
PT	4 days	594.33 ± 83.3 Aab 808.00 ± 15.0 Ac 1183.3 ± 71.8 Bb 596.67 ± 31.3 Aa 23.1
	3 days	$805.33 \pm 58.4 \text{ Ab}$ $755.67 \pm 26.7 \text{ Abc}$ $1214.0 \pm 97.7 \text{ Bb}$ $1184.00 \pm 73.0 \text{ Bc}$ 12.416 .002
	5 days	$466.00 \pm 8.0 \text{ Aa}$ $604.67 \pm 10.7 \text{ Ba}$ $968.67 \pm 21.9 \text{ Cab}$ $641.33 \pm 9.6 \text{ Ba}$ 242.044
UT	4 days	489.67 ± 20.7 Aa 612.00 ± 5.0 Ba 1065.3 ± 32.9 Cab 541.67 ± 6.3 ABa 175.562
	3 days	$456.00 \pm 47.6 ^{\mathrm{Aa}}$ $664.67 \pm 35.7 ^{\mathrm{Bab}}$ $879.00 \pm 15.7 ^{\mathrm{Ca}}$ $880.00 \pm 15.8 ^{\mathrm{Cb}}$ 40.770 .000
		Neat 2 wt.% 3 wt.% 5 wt.% <i>F</i> Signif

Values are in mean \pm standard error. ANOVA (one-way) with Tukey's HSD post hoc test. Means with different letters differ significantly; uppercase letters for vertical comparison and

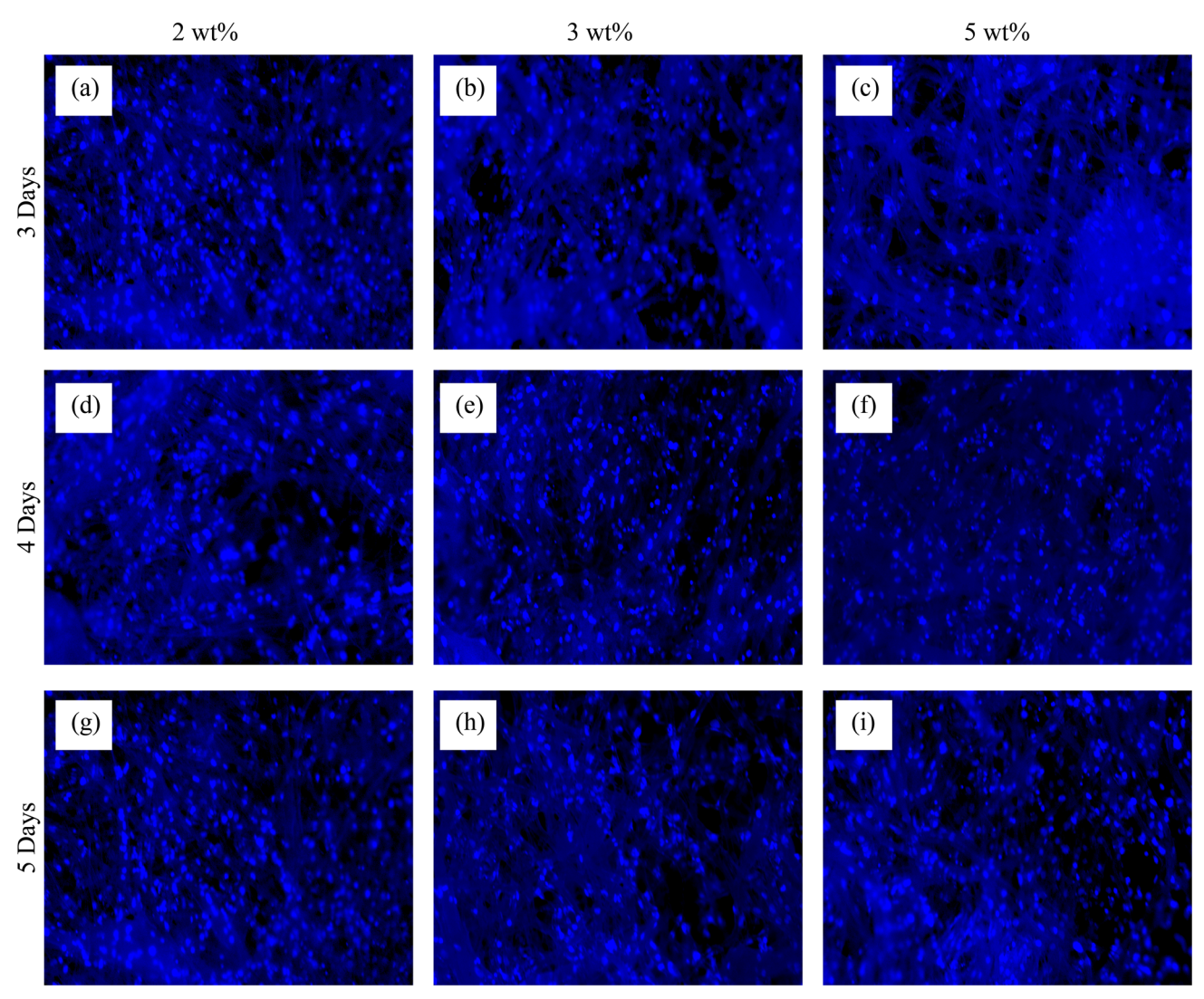


Fig. 7. Photomicrographs of cell adhesion on plasma-treated n-HAp PCL scaffolds for 3 days: (a) 2 wt.%, (b) 3 wt.%, (c) 5 wt.%; 4 days: (d) 2 wt.%, (e) 3 wt.%, (f) 5 wt.%; and 5 days: (g) 2 wt.%, (h) 3 wt.%, and (i) 5 wt.%.

cells grew and masked the micropores, as shown in Fig. 7. The scaffold surfaces are covered with a thin layer of cells after 3 days. All the plasma-treated scaffolds exhibited higher cell numbers when compared to their respective untreated scaffolds. The plasma-treated scaffolds after 3, 4, and 5 days are shown in Fig. 7. The PCL scaffolds infused with 2% wt.% n-HAp and plasma-treated show significantly higher numbers of cell growth from 3 days to 5 days (Table IV and Fig. 7). The plasma-treated scaffolds with 3% n-Hap exhibited a high cell count on the 3rd day, which decreased slightly (non-significantly) by 4th and 5th days. On the other hand, it can be seen that the plasma-treated scaffolds with 5% n-Hap exhibited the highest number of cell attachment on the 3rd day which was significantly decreased by the 4th and 5th days. The low cellular adhesion that is evident by the number of cells on the 5 wt.% when compared to the 2 wt.% and 3 wt.% could be attributed to the low oxygen content in the

5 wt.% plasma-treated scaffolds. The improved oxygen content and other parameters are implicated for better cell counts observed in the 2 and 3 wt.% plasma-treated scaffolds. The cells exhibited excellent attachment for the 2 wt.% plasma-treated scaffolds from day 3, and had full compatibility with the scaffolds, as evidenced by the highest number of cells by the end of the 5th day. A similar growth pattern was observed for the hFOB cells on the 3D-printed scaffolds.³⁷ The DAPI-stained images suggest that these scaffolds can serve as a domain where osteoblasts can grow, attach, and proliferate. The biocompatible HAp obtained from the biomaterials exhibited better biological properties due to the presence of cations, like Mg_2 +, $Zn_2 +$, $Al_3 +$, K +, and Na +, along with anions like Cl- and F-, which are essential for rapid bone regeneration.

CONCLUSION

The n-HAp powder was synthesized from carp fish scales by calcination, and characterized using XRD, SEM, TEM, and XPS. The XRD results suggest that the crystallite size is within the nano-range based on standard HAp. In addition, the SEM and TEM results also demonstrated that the synthesized n-HAp particles are nanosized, have a porous surface, and are irregular. Forcespinning was successfully used to develop n-HAp PCL fibrous scaffolds using centrifugal forces. The influence of the n-HAp content and the plasma treatment on n-HAp PCL scaffolds was investigated. The thermos-mechanical and biological properties were analyzed. The diameter of the fibers increased with the filler content. The plasma treatment induced porosity on the surface of the fibers, which promoted cell adhesion. Despite the improvement in the crystallinity of the fibers with the addition of low filler content, it can be inferred that there is no significant change in the thermal stability of the samples. Plasma treatment also did not induce any thermal stability. The mechanical properties were significantly improved for 3 wt.% samples compared to neat samples, following the crystallinity of the fibers. It is assumed that, with the addition of high filler content, the agglomerates might cause the deterioration of the properties. Nevertheless, observed thermal and mechanical properties are adequate and satisfactory for biomedical applications. The analysis of the cell studies has shown that, with the plasma treatment, cell adhesion and proliferation were significantly improved at low filler contents. Thus, the plasma treatment complements the thermo-mechanical properties of 2 wt.% and 3 wt.% n-HAP fibrous scaffolds with enhanced functionality and biocompatibility. Based on the results of this study, it is suggested that the n-HAp derived from the fish scales can be used for tissue regeneration and wound healing as potential biomedical applications.

SUPPLEMENTARY INFORMATION

The online version contains supplementary material available at https://doi.org/10.1007/s11837-023-05750-5.

ACKNOWLEDGEMENTS

The authors acknowledge financial support from NSF-CREST #1735971, NSF-EPSCoR # 1655280, NSF-RISE # 1459007, NSF-MRI, #1531934 and grant #G12MD007585. The authors also acknowledge Dr. Paul Baker from University of Alabama in Birmingham for his support in XPS studies.

DATA AVAILABILITY

The data that support the findings of this study are available from the corresponding author upon reasonable request.

CONFLICT OF INTEREST

The authors declare no financial or commercial conflict of interest.

REFERENCES

- M. Asadian, K.V. Chan, M. Norouzi, S. Grande, P. Cools, R. Morent, and N. De Geyter, *Nanomaterials* 10, 119 (2020).
- A. Nahanmoghadam, M. Asemani, V. Goodarzi, and S. Ebrahimi-Barough, J. Biomed. Mater. Res. Part A 109, 981 (2021).
- G. Chen and N. Kawazoe, in edited by J. M. Oliveira, S. Pina, R. L. Reis, and J. San Roman (Springer International Publishing, Cham, 2018), pp. 171–191.
- M. Hosseinkhani, D. Mehrabani, M.H. Karimfar, S. Bakhtiyari, A. Manafi, and R. Shirazi, World J. Plast. Surg. 3, 3 (2014)
- A. Chlanda, P. Oberbek, M. Heljak, Z Górecka, K. Czarnecka, K.S. Chen, and M.J. Woźniak, Surf. Coat. Technol. 375, 637 (2019).
- N. Sultana and M. Wang, J. Mater. Sci. Mater. Med. 19, 2555 (2007).
- D. Sin, X. Miao, G. Liu, F. Wei, G. Chadwick, C. Yan, and T. Friis, *Mater. Sci. Eng. C* 30, 78 (2010).
- 8. D.J. Mooney, D.F. Baldwin, N.P. Suh, J.P. Vacanti, and R. Langer, *Biomaterials* 17, 1417 (1996).
- N. Thadavirul, P. Pavasant, and P. Supaphol, J. Biomed. Mater. Res. Part A 102, 3379 (2014).
- O.A. Abdelaal and S.M. Darwish, J. World Acad. Sci. Eng. Technol. 59, 577 (2011).
- S.N. Gorodzha, A.R. Muslimov, D.S. Syromotina, A.S. Timin, N.Y. Tcvetkov, K.V. Lepik, A.V. Petrova, M.A. Surmeneva, D.A. Gorin, G.B. Sukhorukov, and R.A. Surmenev, Colloids Surf. B Biointerfaces 160, 48 (2017).
- T.A. Vida, A.C. Motta, A.R. Santos, G.B.C. Cardoso, C.C. De Brito, and C.A. De Carvalho Zavaglia, *Mater. Res.* 20, 910 (2017).
- J.F. Kim, J.H. Kim, Y.M. Lee, and E. Drioli, AIChE J. 62, 461 (2016).
- 14. S. Zhang, Nat. Biotechnol. 21, 1171 (2003).
- M. Cámara-Torres, R. Sinha, P. Scopece, T. Neubert, K. Lachmann, A. Patelli, C. Mota, L. Moroni, and A.C.S. Appl, Mater. Interfaces 13, 3631 (2021).
- Q. Cheng, B.L.P. Lee, K. Komvopoulos, Z. Yan, and S. Li, Tissue Eng. Part A 19, 1188 (2013).
- M. Rampichová, M. Buzgo, J. Chvojka, E. Prosecká, O. Kofronová, and E. Amler, Cell Adhes. Migr. 8, 36 (2014).
- V. Padilla-Gainza, G. Morales, H. Rodriguez-Tobías, and K. Lozano, J. Appl. Polym. Sci. 136, 1 (2019).
- 19. Z. McEachin and K. Lozano, *J. Appl. Polym. Sci.* 126, 473 (2011)
- K. Sarkar, C. Gomez, S. Zambrano, M. Ramirez, E. De Hoyos, H. Vasquez, and K. Lozano, *Mater. Today* 13, 12 (2010).
- F. Asghari, M. Samiei, K. Adibkia, A. Akbarzadeh, and S. Davaran, Artif. Cells Nanomed. Biotechnol. 45, 185 (2017).
- K. Del Ángel-Sánchez, N.A. Ulloa-Castillo, E. Segura-Cárdenas, O. Martinez-Romero, and A. Eliás-Zuñiga, MRS Commun. 9, 390 (2019).
- A.A. Ivanova, D.S. Syromotina, S.N. Shkarina, R. Shkarin, A. Cecilia, V. Weinhardt, T. Baumbach, M.S. Saveleva, D.A. Gorin, T.E.L. Douglas, B.V. Parakhonskiy, A.G. Skirtach, P. Cools, N. De Geyter, R. Morent, C. Oehr, M.A. Surmeneva, and R.A. Surmenev, RSC Adv. 8, 39106 (2018).

Enhancement of Biocompatibility of Fish Scale-Based Hydroxyapatite-Infused Fibrous Scaffolds by Low-Temperature Plasma

- Z. Mohammed, S. Jeelani, and V. Rangari, JOM 72, 1523 (2020).
- P. Chocholata, V. Kulda, and V. Babuska, Materials (Basel) 12, 568 (2019).
- P. Palmero, Ceramic-polymer nanocomposites for bone-tissue regeneration, in Nanocomposites for Musculoskeletal Tissue Regeneration. (Elsevier, 2016), pp. 331–367. https://doi.org/10.1016/B978-1-78242-452-9.00015-7.
- 27. C.I. Idumah, Polym. Polym. Compos. 29, 509 (2020).
- N.G. Sahoo, Y.Z. Pan, L. Li, and C. Bin He, *Nanomedicine* 8, 639 (2013).
- S. Park, J.E. Kim, J. Han, S. Jeong, J.W. Lim, M.C. Lee, H. Son, H.B. Kim, Y.H. Choung, H. Seonwoo, J.H. Chung, and K.J. Jang, *Polymers (Basel)* 13, 1 (2021).
- R.M. Mohamed and K. Yusoh, Adv. Mater. Res. 1134, 249 (2016).
- S. Sathiskumar, S. Vanaraj, D. Sabarinathan, S. Bharath,
 G. Sivarasan, S. Arulmani, K. Preethi, and V.K. Ponnusamy, Ceram. Int. 45, 7804 (2019).
- N.A.S. Mohd Puad, R.H. Abdul Haq, H. Mohd Noh, H.Z. Abdullah, M.I. Idris, and T.C. Lee, *Mater. Today Proc.* 29, 218 (2019).
- S. Mondal, G. Hoang, P. Manivasagan, M.S. Moorthy, H.H. Kim, T.T. Vy Phan, and J. Oh, *Mater. Chem. Phys.* 228, 344 (2019).
- P. Surya, A. Nithin, A. Sundaramanickam, and M. Sathish, J. Mech. Behav. Biomed. Mater. 119, 104501 (2021).
- 35. M.R. Hasan, S.N. Mohd Yasin, M.S. Mohd Ghazali, and N.F. Mohtar, J. Sustain. Sci. Manag. 15, 9 (2020).
- A. Pal, S. Maity, S. Chabri, S. Bera, A.R. Chowdhury, M. Das, and A. Sinha, *Biomed. Phys. Eng. Express* 3, 15010 (2017).
- V. Hembrick-Holloman, T. Samuel, Z. Mohammed, S. Jeelani, and V.K. Rangari, J. Mater. Res. Technol. 9, 13729 (2020).
- and V.K. Rangari, J. Mater. Res. Technol. 9, 13729 (2020) 38. Y. Chai and M. Tagaya, Mater. Lett. 222, 156 (2018).
- 39. E. Barua, A.B. Deoghare, P. Deb, S. Das Lala, and S. Chatterjee, *Mater. Today Proc.* 15, 188 (2019).
- D. Kodali, V. Hembrick-Holloman, and S. Jeelani, V. K. Rangari, in *Plant Anim. Based Compos.* ed. by K. Kumar, and J.P. Davim (De Gruyter, Berlin, Boston, 2021), pp. 127–148.
- 41. J. Sawai, Biocontrol Sci. 16, 95-102 (2011).
- W.-K. Liu, B.-S. Liaw, H.-K. Chang, Y.-F. Wang, and P.-Y. Chen, *JOM* 69, 713 (2017).
- S. Paul, A. Pal, A.R. Choudhury, S. Bodhak, V.K. Balla, A. Sinha and M. Das. Ceram. Int. 43, 15678 (2017)
- Sinha, and M. Das, *Ceram. Int.* 43, 15678 (2017). 44. C.S. Wu, D.Y. Wu, S.S. Wang, and A.C.S. Appl, *Bio Mater.* 4,
- 462 (2021).45. N.I. Agbeboh, I.O. Oladele, O.O. Daramola, A.A. Adediran, O.O. Olasukanmi, and M.O. Tanimola, *Heliyon* 6, e03765
- H. Yamamura, V.H.P. da Silva, P.L.M. Ruiz, V. Ussui, D.R.R. Lazar, A.C.M. Renno, and D.A. Ribeiro, J. Mech. Behav. Biomed. Mater. 80, 137 (2018).
- P. Deb, A.B. Deoghare, E. Barua, and I.O.P. Conf, Ser. Mater. Sci. Eng. 377, 012009 (2018).
- P. Deb, E. Barua, A.B. Deoghare, and S. Das Lala, Ceram. Int. 45, 10004 (2019).
- N.P. Wijedasa, S.M. Broas, R.E. Daso, and I.A. Banerjee, *Mater. Sci. Eng. C* 109, 110540 (2020).
- S. Jin, F. Sun, Q. Zou, J. Huang, Y. Zuo, Y. Li, S. Wang, L. Cheng, Y. Man, F. Yang, and J. Li, *Biomacromolcules* 20, 2058 (2019).

- L. Li, Y. Zuo, Q. Zou, B. Yang, L. Lin, J. Li, Y. Li, and A.C.S. Appl, *Mater. Interfaces* 7, 22618 (2015).
- S.Y. Heo, S.C. Ko, G.W. Oh, N. Kim, I.W. Choi, W.S. Park, and W.K. Jung, J. Biomed. Mater. Res. Part B Appl. Biomater. 107, 1937 (2019).
- W. Pon-On, P. Suntornsaratoon, N. Charoenphandhu, J. Thongbunchoo, N. Krishnamra, and I.M. Tang, *Mater. Lett.* 221, 143 (2018).
- B. Vandana, P. Syamala, D.S. Venugopal, S.R.K.I. Sk, B. Venkateswarlu, M. Jagannatham, M. Kolenčík, I. Ramakanth, R. Dumpala, and B.R. Sunil, *Bull. Mater. Sci.* 42, 122 (2019).
- P.N. Sivasankaran and T.A. Ward, Aerosp. Sci. Technol. 49, 259 (2016).
- H.S. Yoo, T.G. Kim, and T.G. Park, Adv. Drug Deliv. Rev. 61, 1033 (2009).
- N. Recek, M. Resnik, H. Motaln, T. Lah-Turnšek, R. Augustine, N. Kalarikkal, S. Thomas, and M. Mozetič, *Int. J. Polym. Sci.* 2016, 1–9 (2016).
- J. Venugopal, S. Low, A.T. Choon, A.B. Kumar, and S. Ramakrishna, J. Biomed. Mater. Res. Part A 85A, 408 (2008).
- C.-M. Lee, S.-W. Yang, S.-C. Jung, and B.-H. Kim, J. Nanosci. Nanotechnol. 17, 2747 (2017).
- D. Kodali, V. Hembrick-Holloman, D.R. Gunturu, T. Samuel, S. Jeelani, and V.K. Rangari, ACS Omega 7, 8323 (2022).
- D. Kodali, F. Syed, S. Jeelani, and V.K. Rangari, *Mater. Res. Express* 7, 125402 (2020).
- 62. M.P. Prabhakaran, J. Venugopal, C.K. Chan, and S. Ramakrishna, *Nanotechnology* 19, 455102 (2008).
- A.M. Pappa, V. Karagkiozaki, S. Krol, S. Kassavetis, D. Konstantinou, C. Pitsalidis, L. Tzounis, N. Pliatsikas, and S. Logothetidis, *Beilstein J. Nanotechnol.* 6, 254 (2015).
- D. Xu, B. Liu, G. Zhang, S. Long, X. Wang, and J. Yang, *High Perform. Polym.* 28, 411 (2016).
- B. Huang, G. Caetano, C. Vyas, J.J. Blaker, C. Diver, and P. Bártolo, *Materials (Basel)* 11, 129 (2018).
- M. Sivan, D. Madheswaran, M. Asadian, P. Cools, M. Thukkaram, P. Van Der Voort, R. Morent, N. De Geyter, and D. Lukas, Surf. Coat. Technol. 399, 126203 (2020)
- and D. Lukas, Surf. Coat. Technol. 399, 126203 (2020).
 67. A. Esmail, J.R. Pereira, P. Zoio, S. Silvestre, U.D. Menda, C. Sevrin, C. Grandfils, E. Fortunato, M.A.M. Reis, C. Henriques, A. Oliva, and F. Freitas, Polymers (Basel). 13, 1 (2021).
- V. Trakoolwannachai, P. Kheolamai, and S. Ummartyotin, Compos. Part B Eng. 173, 106974 (2019).
- M.A. Taghavi, S.M. Rabiee, M. Jahanshahi, and F. Nasiri, Mol. Biotechnol. 61, 345 (2019).

Publisher's Note Springer Nature remains neutral with regard to jurisdictional claims in published maps and institutional affiliations.

Springer Nature or its licensor (e.g. a society or other partner) holds exclusive rights to this article under a publishing agreement with the author(s) or other rightsholder(s); author self-archiving of the accepted manuscript version of this article is solely governed by the terms of such publishing agreement and applicable law.